ELSEVIER

Contents lists available at ScienceDirect

Electrochimica Acta

journal homepage: www.journals.elsevier.com/electrochimica-acta



Exploring environmentally friendly localised corrosion inhibitors through local electrochemical measurements using multielectrode arrays

Medhani Pathirana ^a, Majid Laleh ^{a,b}, Anthony Somers ^c, Bruce Hinton ^c, GlenB. Deacon ^d, PeterC. Junk ^e, MikeYongjun Tan ^{a,c,*}

- ^a School of Engineering, Deakin University, Waurn Ponds, VIC 3216, Australia
- ^b ARC Research Hub for Australian Steel Innovation, University of Wollongong, Wollongong, NSW 2522, Australia
- Institute for Frontier Materials, Deakin University, Waurn Ponds, VIC 3216, Australia
- ^d School of Chemistry, Monash University, Clayton Campus, VIC 3800, Australia
- ^e College of Science & Engineering, James Cook University, Townsville, Qld 4811, Australia

ARTICLE INFO

Keywords: Corrosion inhibitor Localised corrosion Waterline corrosion Electrochemical measurements Steel Multi-electrode array Rare earths

ABSTRACT

Localised corrosion is the result of complex heterogeneous electrochemical processes occurring on metal surfaces. Localised corrosion control is one of the most difficult issues in corrosion science and engineering. This study reports a new approach to exploring effective and environmentally friendly localised corrosion inhibitors through local electrochemical measurements using multielectrode array probes. Local galvanic current, local polarisation, and local electrochemical impedance spectroscopy (EIS) measurements were performed on an electrode array probe exposed to waterline corrosion conditions, with and without the presence of rare earth metal (REM) inhibitors that are known to be effective for inhibiting general corrosion. The results revealed significant differences in the behaviour of two REM inhibitors, with La(40Hcin) $_3$ ·5H $_2$ O exacerbating localised corrosion by generating intense anodic sites with high local corrosion current densities, while [Y(mbp) $_3$ ·H $_2$ O] showing the ability of inhibiting localised corrosion. Such localised corrosion inhibition ability by [Y(mbp) $_3$ ·H $_2$ O] was found to be associated with the formation of an inhomogeneous surface film that allows the existence of minor anodes randomly distributing over the surface, leading to low anodic current densities and insignificant general corrosion rather than severe localised corrosion. These results demonstrate a new approach to discovering localised corrosion inhibitors through local electrochemical measurements using electrode arrays.

1. Introduction

In electrochemical reactions the reactants do not need to be spatially near each other, as normal chemical reactions do, they collide separately with spatially separated metal surface areas, permitting distinct separation of electrode reactions over an electrode surface and therefore the localisation of electrochemical processes such as localised corrosion. Localised corrosion is a critical issue that often causes premature failure of engineering structures, especially those exposed to complex and corrosive environments. In industry, corrosion-induced failures are frequently driven by localised forms of corrosion, which lead to deep penetration and local structural weakening, particularly at stress-concentration sites where fractures can initiate [1,2]. One of the most difficult forms of localised corrosion is waterline corrosion that poses major challenges to structures exposed to air/liquid interfaces, such as

shore-crossing pipelines, offshore wind turbines, and marine platforms. Numerous historical cases have documented waterline corrosion on ship hulls, steel pilings, ballast tanks, and liquid storage tanks [3–7]. The current understanding attributes waterline corrosion mainly to galvanic activity driven by oxygen concentration cells, where the highly oxygenated regions above the waterline act as cathodes and the poorly oxygenated submerged regions become anodic [8–11]. Recently the formation of rust layers was found to be another important factor affecting waterline corrosion by forming crevice-like environments, accelerating localised corrosion beneath the rusted steel surface [10–12].

Developing effective methods and materials to control localised corrosion such as waterline corrosion is vital for protecting infrastructure operating under challenging and variable environmental conditions. Chemical inhibitors are widely used in corrosion control due to

E-mail address: mike.tan@deakin.edu.au (M. Tan).

^{*} Corresponding author.

their flexibility, practicality, and cost-effectiveness. Some inhibitors such as scavengers like hydrazine, biocides like glutaraldehyde, and scale inhibitors like phosphonates [13-17] mitigate corrosion by altering or modifying local environmental conditions. Some other inhibitors including chromates, nitrites, molybdates, phosphates, gluconates, nitrates, and sulphates mitigate corrosion by impeding corrosion reaction kinetics. Some of these inhibitors have shown varying degrees of effectiveness in mitigating both general and localised corrosion [18–24], however most of these inhibitors suffer from limited reliability, concentration sensitivity, and environmental toxicity. Notably, compounds like chromates and nitrites are effective corrosion inhibitors but are considered to be hazardous and unreliable, particularly if applied below threshold concentrations. In recent decades, rare earth metal (REM) inhibitors have gained interest as safer and more sustainable alternatives. Early work by Hinton et al. showed that CeCl3 reduced mild steel corrosion in water through protective film formation [25,26]. Later studies found that organic ligands such as cinnamic acid could enhance anodic inhibition [27]. Forsyth et al. introduced REM carboxylates as mixed inhibitors that suppress both anodic and cathodic reactions across metal surfaces [28], and other researchers have expanded on this by developing REM-organic complexes with improved surface bonding [29–39]. While most of these studies have focused on general corrosion, some REM inhibitors have demonstrated promise for mitigating localised corrosion on aluminium alloys via cathodic site precipitation [35,

Despite these advances, two major issues remain unaddressed: (i) the lack of effective inhibitors that reliably suppress severe localised corrosion under real-world conditions, such as at waterlines; and (ii) the lack of convenient and efficient experimental method that can be used for discovering effective, non-toxic and environmentally friendly localised inhibitors. This study aims to address both issues by investigating the waterline corrosion inhibition performance of two REM-organic compounds, i.e., La(4OHcin)₃·5H₂O and [Y(mbp)₃·H₂O], using a new experimental approach. These REM inhibitors are selected because they have shown high efficiency in mitigating general corrosion of steel [40-42] but remained underexplored for localised corrosion control. In this work, we used local electrochemical techniques based on an electrochemically integrated multielectrode array namely the Wire Beam Electrode (WBE), which allows in-situ monitoring of galvanic currents, local polarisation, and local electrochemical impedance spectroscopy (EIS). Unlike conventional techniques that measure averaged corrosion behaviour, the WBE captures spatial variations in electrochemical activities and corrosion dynamics [10,11]. Our previous work using this method revealed the critical role of rust in modifying local electrochemistry at the waterline [10]. This study builds on that by using the WBE to measure and evaluate inhibitor performance and its changes over time under waterline conditions, and to probe the mechanisms of localised corrosion inhibition.

2. Materials and methods

The electrode array probe used in this work consisted of 100 square electrodes (electrode dimensions 2.3 mm \times 2.3 mm). The electrodes were made from X65 carbon steel (composition of 0.04 C, 0.2 Si, 1.5 Mn, 0.011 P, 0.003 S, 0.02 Mo, and Fe balance (wt%)). The100 electrodes were all mounted in epoxy and arranged in an array of 25 rows with 4 per row. The 100 electrodes of the multi-electrode array were electrically connected to simulate a continuous steel surface. To simulate the waterline corrosion conditions, the array was partially immersed in the test solution such that 6 rows of the array were exposed to air (above waterline) and 19 rows below waterline. This setup allows continuous monitoring of corrosion over the array surface for long exposure times and enables detection of corrosion at local areas of the electrode array. This setup is considered as an improved method to study localised corrosion as it can overcome limitations of conventional methods of studying waterline corrosion as described in our previous papers [10,2].

While it is recognised that the corners of square-shaped electrode array could exhibit enhanced local current density due to geometric effects, preferential corrosion activity at the corners of the electrode array was not observed in this work. This is because waterline corrosion on the electrode array surface was mainly controlled by significant galvanic activities driven by major oxygen concentration cells at the air/solution interface, where the highly oxygenated regions above the waterline act as cathodes and the poorly oxygenated submerged regions become anodic [8–11]. The geometric effect at the corners of the electrode array was only a minor influencing factor. The corrosion behaviour observed on the electrode array was consistently aligned with those reported in the literature [8–11]. This experimental method addresses a major challenge in the rapid evaluation of localised corrosion inhibitor performance.

Before each experiment, the surface of electrode array probe was ground using SiC abrasive papers down to 1200 grit finish, cleaned with ethanol and dried with hot air. A 3.5 wt% NaCl solution (pH \sim 7) was used as the control solution (without any inhibitor) for comparison of corrosion pattern and mechanism. For the studies with inhibitor present, either 1 mmol/l of La(40Hcin) $_3$ -5H $_2$ O (solubility is 1.34 mmol/l) or 1 mmol/l of [Y(mbp) $_3$ -H $_2$ O] (solubility 0.25 mmol/l, so reservoir of solid to maintain saturation) was added to the control solution to ensure that a saturated solution was prepared. These were prepared according to the literature [43,44]. Fresh solutions were used for each replicate experiment. Volume of the test solution for each experiment was 3 litres. To overcome the evaporation and to maintain the waterline in the same position, distilled water was added periodically. All experiments were conducted for 14 days under static conditions at room temperature.

Galvanic current distribution mapping was carried out continuously during the experiment for various periods. Each current measurement cycle for 100 electrodes took almost 5 min. Based on these galvanic current maps, local anodic and cathodic sites could be identified, with positive and negative currents representing anodic and cathodic currents, respectively. By summing up all the positive currents, total anodic currents were calculated. Localised corrosion rates and localised corrosion depths were calculated using Eqs. (1) and (2). The localised corrosion depth value was calculated for each day and the summation of all corrosion depth values provided as the accumulated corrosion depth.

Localised corrosion rate
$$= K \frac{i_{corr(i)}}{\rho} EW \text{ (mm / y)}$$
 (1)

Where K is constant $(3.27 \times 10^{-3} \text{ mm g/µA cm y})$, ρ is the density of X65 steel (7.8 g/cm³), $i_{corr(i)}$ is the galvanic current at ith electrode and EW is equivalent weight for X65 steel (27.92).

Localised corrosion depth
$$= \frac{\textit{LCR} \times 1000 \times \textit{Period}}{24 \times 365} (\mu\text{m})$$
 (2)

Where LCR is the localised corrosion rate measured from Eq. (1), and Period is the exposure time (for this study is 24 h). For accumulated corrosion depth measurements, localised corrosion rate was assumed to be constant during the exposure period of 24 h.

For the inhibition mechanism and efficiency studies, local potentiodynamic polarisation and EIS measurements were carried out, which provided information about the local electrochemical behaviour and changes at local cathodic and anodic sites. Local polarisation measurements at individual electrodes were carried out after 14 days of testing in the solution with REM carboxylate inhibitor. For these experiments, each individual electrode of interest was electrically disconnected from the array electrode and connected to the potentiostat as the working electrode. Ag/AgCl electrode was used as the reference electrode and a Pt-coated Ti mesh was used as the counter electrode. For individual electrodes with positive currents (i.e., anodic sites), the potential was swept from 50 mV below the open circuit potential (OCP) to 300 mV above the OCP. For individual electrodes with negative currents (i.e., cathodic sites), the potential was swept from 300 mV below the OCP to 50 mV above the OCP at 1mV/sec scan rate. During each local

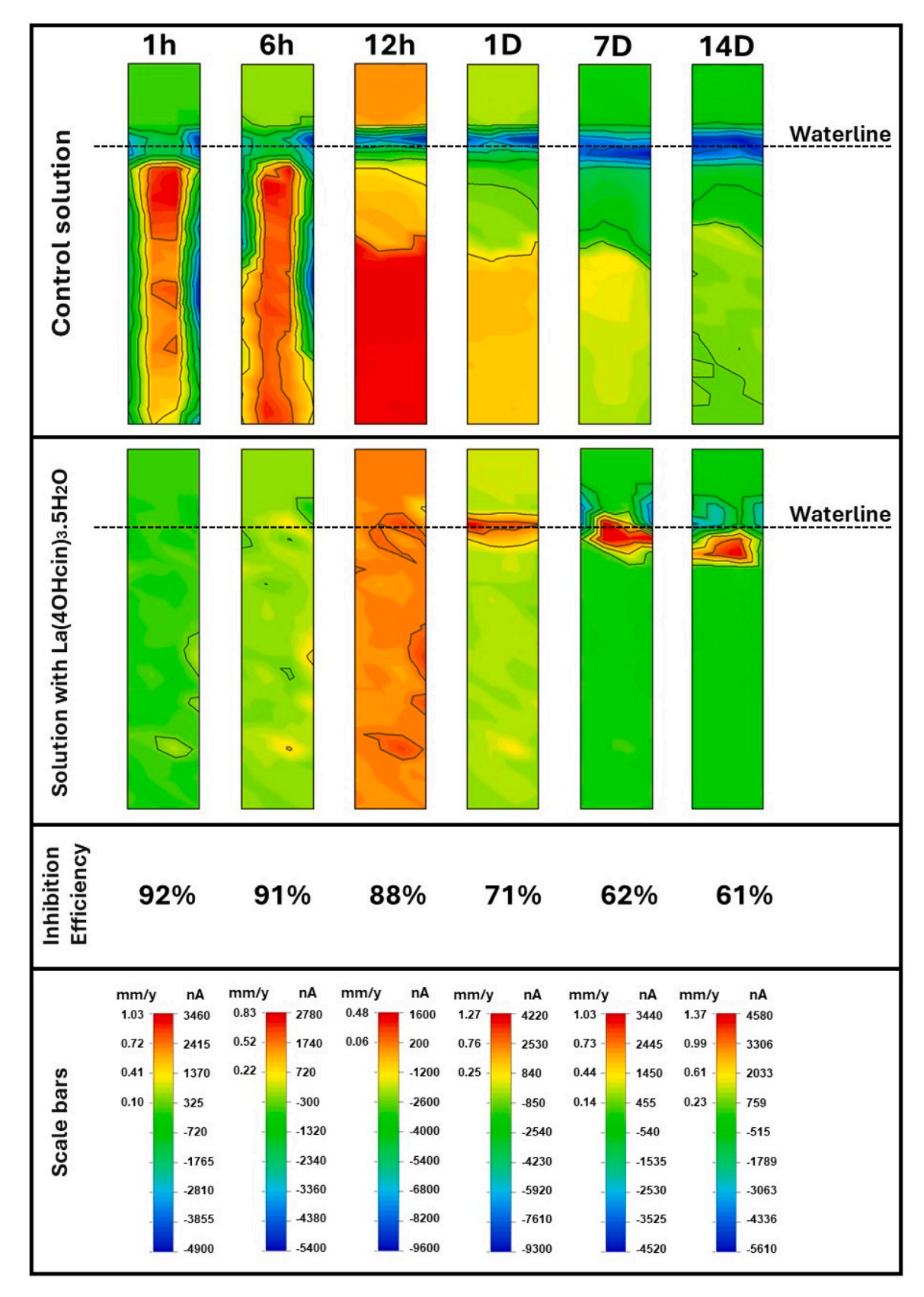


Fig. 1. Galvanic current maps obtained from multi electrode arrays which exposed to the control solution (3.5 wt% of NaCl) and to the solution containing La $(40Hcin)_3 \cdot 5H_2O$ after different periods of exposure.

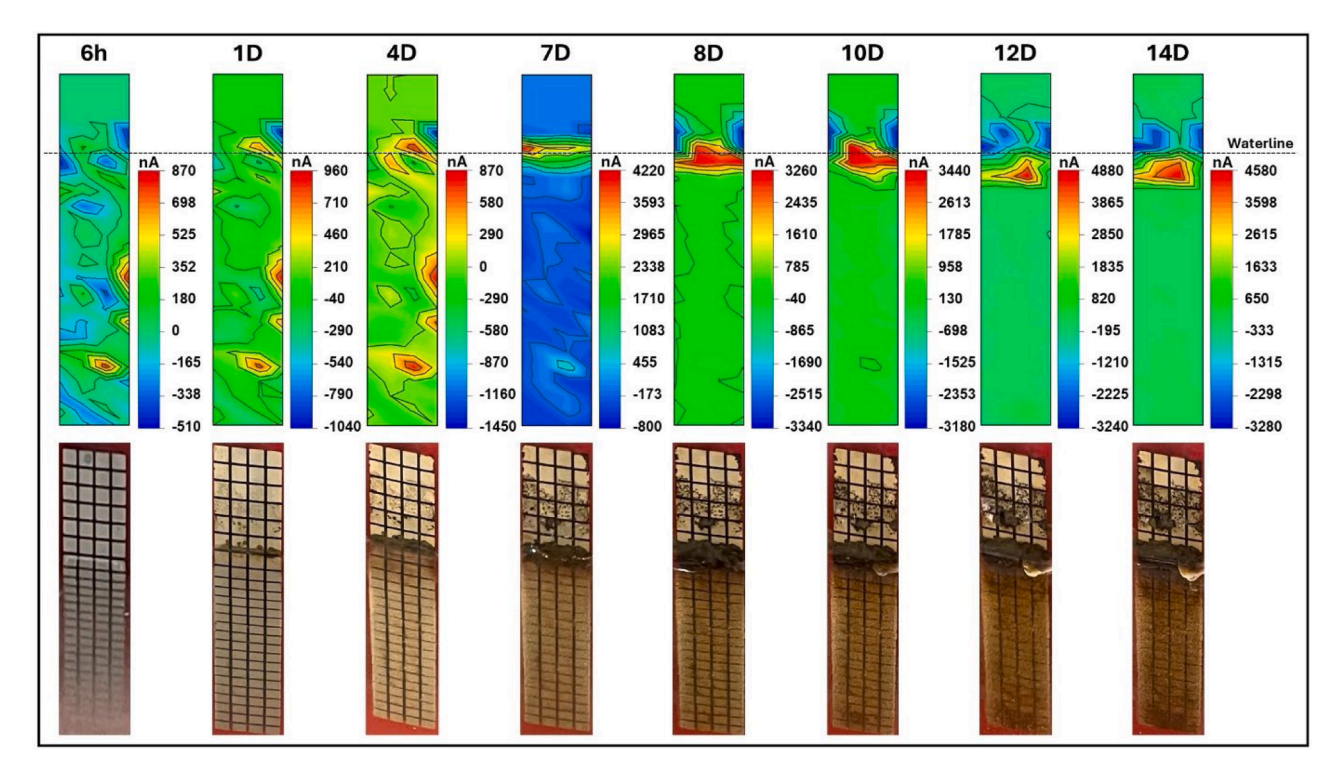


Fig. 2. Representative galvanic current maps along with photographs of the electrode array that was partially exposed to the solution containing 1 mmol/l La (40Hcin)₃·5H₂O at different exposure times under static conditions. Note that individual scale bars are used for each map.

polarisation measurement, potential range was decided carefully such that the potential range is large enough to show electrochemical changes due to inhibitors and also the potential range is small enough to minimise the damage to the steel surface due to polarisation measurements. More details on the galvanic current mapping and local polarisation measurements can be found in our previous works [1,2]. Local electrochemical impedance spectroscopy (EIS) measurements were also performed at each selected individual electrode in a frequency range from 100 kHz to 10 mHz. To draw local EIS maps, local film resistance values across the whole probe were estimated by Nyquist plots fitting. All electrochemical measurements were carried out using a Bio-Logic VSP multi-channel potentiostat and were analysed using EC-Lab Software V11.36.

Fourier transform infrared spectroscopy (FTIR) was performed to analyse the composition of the films (deposits) formed on the electrode array surface in two ways: (i) a general information was obtained by performing the FTIR test on the deposit acquired from the whole electrode surface, and (ii) a *site-specific* information was obtained by performing the FTIR test on the deposit acquired from intended individual electrode. The latter allows identifying the compositional differences between films formed on anodic sites versus those formed on cathodic sites. For the FTIR tests, PerkinElmer Frontier spectrometer with a diamond attenuated total reflectance (ATR) crystal 64 scans across the 4000–650 cm⁻¹ wavelength was used.

3. Results and discussion

A series of experiments have been conducted to understand the effects of different REM carboxylate inhibitors on waterline corrosion and on the localisation of electrochemistry over locally corroding metal surfaces partially immersed in corrosive aqueous media with 3.5 wt% NaCl solution (pH \sim 7) as the control solution.

3.1. Effects of REM inhibitors on waterline corrosion

Experiments were carried out to evaluate the efficiency of a typical

REM carboxylate corrosion inhibitor La(40Hcin)₃·5H₂O under simulated waterline corrosion conditions. Fig. 1 shows time-lapse galvanic current maps of the electrode array probe exposed to the control solution with addition of 1 mmol/l of La(4OHcin)3.5H2O. Using the current values from each map, total anodic current (summation of positive current values at local anodes), overall corrosion rate (calculated using Eq. (1) considering the whole electrode array as a single electrode with the area of 3.61 cm²) and inhibition efficiency (percentage reduction of total anodic current) were calculated. In the presence of La (4OHcin)₃·5H₂O, total anodic current after 1 h of exposure was measured to be 6563 nA, which is significantly lower than that measured in the control solution (84,430.2 nA). The total anodic current is directly related to corrosion rates, and this drop in total anodic current suggests a 92% efficiency for this inhibitor. This inhibition efficiency is similar to the 91% inhibition efficiency reported in the literature obtained with steel specimens fully immersed in a 0.01 M NaCl solution [40]. Even after 6 h and 12 h of exposure, the inhibition efficiencies in the presence of La(40Hcin)₃·5H₂O were still measured to be 91% and 88%, respectively. Therefore, this result suggests that, at the early stage of exposure, La(4OHcin)3.5H2O was able to efficiently inhibit waterline corrosion on the partially submerged electrode array probe.

With increasing the exposure period to 24 h, total anodic current shows a significant increase from 7977.4 nA to 19,056.6 nA, hence a decrease in inhibition efficiency from 88% to 71%. More importantly, a major anodic area appeared in the galvanic current maps with anodic currents up to 4220 nA and corrosion rates up to 1.27 mm/y. Such localisation of anodic current is not acceptable because localised corrosion is more harmful than general corrosion. Unfortunately, as shown in Fig. 1, the major anodic area with large anodic current remained at the same location near the waterline over 7 and 14 days of exposure, leading to further decrease in inhibition efficiency to 62% and 61%, respectively. This indicates that major and stable local anodes formed over the electrode array surface, which in turn leading to a significant localised corrosion at those major anodic sites adjacent to the cathodic areas at waterline. After 14 days of exposure, the total anodic current was measured to be 19,574.7 nA with an inhibition efficiency of

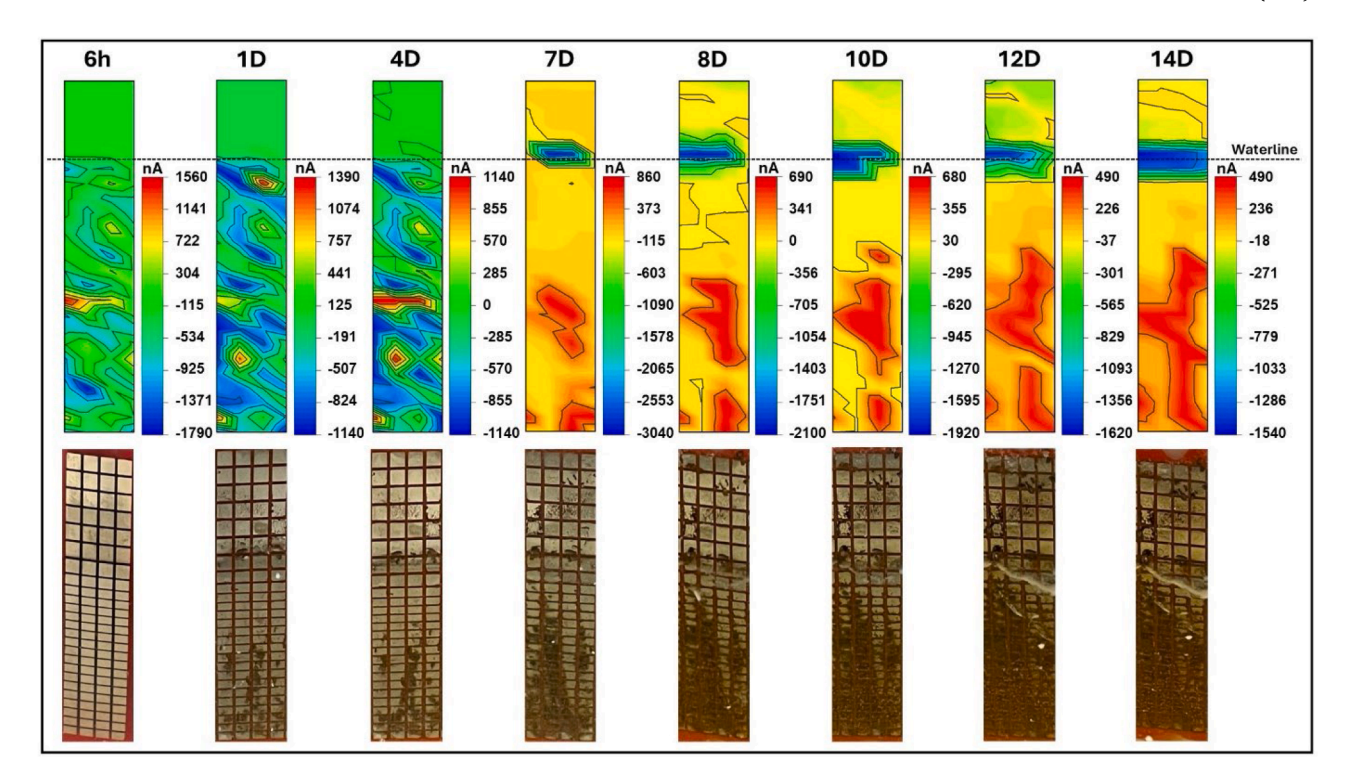


Fig. 3. Galvanic current maps along with photographs of the electrode array exposed to a solution containing 1 mmol/l of [Y(mbp)₃.H₂O].

61%, indicating that La(40Hcin) $_3$ ·5H $_2$ O was still able to mitigate overall corrosion except at the concentrated anodic area where significantly high corrosion occurred. The formation of concentrated active anodes is not acceptable because continuous and rapid anodic dissolution at fixed anodic locations would result in pitting corrosion that is even more damaging than general corrosion that occurs in the inhibitor-free control solution. Fig. 1 indicates that although significantly high metal losses occurred in the inhibitor-free control solution, corrosion penetration rate is lower than that in the solution containing La(40Hcin) $_3$ ·5H $_2$ O.

To further examine the formation of the concentrated anodic sites (localised corrosion) in solution containing La(40Hcin)3:5H2O in more detail, galvanic current maps are represented in Fig. 2 (Note that these maps have individual scales and therefore different colour codes). After 6 h of exposure, a random distribution of anodic and cathodic areas over the probe surface is observed. Although some cathodic sites appear near the waterline, those are not concentrated at waterline (such as that observed for the control solution in Fig. 1), indicating that a significant oxygen differential cell has not been establshed yet at this stage. However after 1 day of exposure, a significant cathodic site was started to form near and at the waterline with anodic sites formed just below the waterline. After 4 days, there is a major cathodic site at and above the waterline with concentrated anodic site just below the waterline, indicating the initiation of a major oxygen differential cell. The concentrated anodic site remained unchanged just below the waterline (pushed a bit down by the formation of major cathodic site) for the remaining exposure time until day 14. Obviously the high general corrosion rates in the inhibitor-free solution (see Fig. 1) and the high localised corrosion at major anodes in the inhibited solution (see Figs. 1 and 2) are both not desirable for effective control of waterline corrosion. These suggest the need to explore ways of inhibiting both general and localised corrosion.

Fig. 2 also shows the photographs of the electrode array surface at each day of exposure to the inhibited solution with La(40Hcin)₃·5H₂O. As can be seen, the concentrated anode can be identified at the waterline in black colour. At the bottom areas of the electrode array, a white colour deposit can be seen by naked eye and this may be the inhibitor-assissted layer. More interestingly, this white colour deposit was not found at the waterline where the concentrated anode was formed.

According to Fig. 1, the corrosion rate at bottom areas of the probe where the white colour deposit formed is as low as 0.01 mm/y, suggesting the formation of a protective film on the surface. Such a protective film might be formed due to the presence of inhibitor in the solution, which will be further examined in Section 3.3.

3.2. A new inhibitor for mitigating localised corrosion at waterline

In severe localised corrosion conditions such as that occuring at waterline, where significant galvanic corrosion environments exist, thermodynamically it is considerred impractical to fully prevent corrosion. A practical approach to mitigating corrosion in such serious and thermodynamically spontaneous waterline corrosion conditions is to reduce general corrosion and, more importantly, at the same time to avoid the formation of dominating local corrosion anodes. This could be achieved by identifying inhibitors that can prevent the formation of major localised anodes by allowing a large number of minor anodes to develop randomly over the steel surface, and therefore leading to less significant anodic dissolution. For instance, Resorcinarene acid was found to have this ability for CO2 corrosion of steel which was fully immersed in CO₂ saturated brine solution [43]. To evaluate this possibility, a newly synthesised REM inhibitor, [Y(mbp)₃.H₂O], was assessed for its ability of inhibiting localised corrosion at waterline. Peng et al. discovered that [Y(mbp)3.H2O] shows better inhibition efficiency for general corrosion compared to La(4OHcin)3·5H2O after longer periods of immersion [42].

Fig. 3 shows galvanic current maps obtained from an electrode array exposed to a 3.5 wt% NaCl (pH \sim 7) solution containing 1 mmol/l of [Y (mbp) $_3$.H $_2$ O]. As can be seen, cathodic and anodic sites are randomly distributed over the electrode array surface after 6 h, 1 day, and 4 days of exposure, indicating that the oxygen differential cell has not been established till this stage of exposure. Although a significant cathodic site was formed after 7 days of exposure and persisted till the end of experiment (14 days), there was no dominating anodic site observable adjacent to the cathodic area at the waterline throughout the 14 days. Some anodic sites appeared at the bottom areas of the probe, however, these anodic areas are distributed rather randomly over the electrode

Table 1Total anodic current and inhibition efficiency after exposing to different solutions for various perdis of time.

Exposure time	Control solution (3.5 wt% NaCl) Total anodic current (nA)	Solution containing La $(4OHcin)_3.5H_2O$		Solution containing [Y (mbp) _{3.} H ₂ O]	
		Total anodic current (nA)	Inhibition efficiency (%)	Total anodic current (nA)	Inhibition efficiency (%)
1 h	84,430.2	6577.4	92	6968.1	92
6 h	80,744.9	7540.0	91	7358.9	91
12 h	67,909.5	7977.4	88	8858.9	87
24 h	66,609.1	19,056.6	71	9356.4	86
7 days	48,419.0	18,546.6	62	10,197.6	79
14 days	49,724.3	19,574.7	61	12,010.1	76

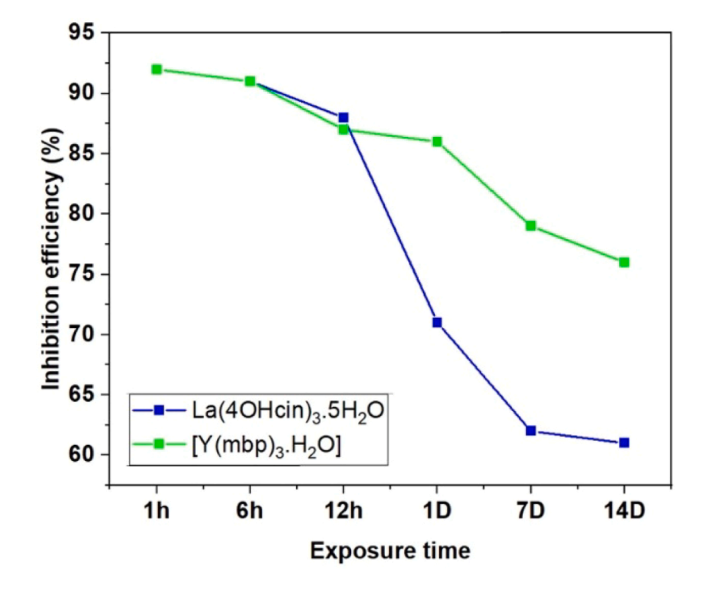


Fig. 4. Inhibition efficiency vs exposure time for solutions containing La $(4OHcin)_3$ - SH_2O (blue curve) and $[Y(mbp)_3$ - $H_2O]$ (green curve).

array surface. Furthermore, from day 1 onwards, it can be visuallay observed that the area of the anodic sites increased. This suggests that this inhibitor impeded the formation of concentrated and dominating anodes by allowing a large number of minor anodes to develop randomly over the steel surface, and therefore leading to less significant concentrated anodic dissolution. On the other hand, as shown in Table 1, the new inhibitor [Y(mbp)₃.H₂O] also reduced general/overall anodic currents compared with those measured from electrode array exposed to either control solution or solution containing La(40Hcin)₃·5H₂O. Fig. 3 also shows time-lapse photographs of the electrode array surface exposed to a solution containing [Y(mbp)3.H2O]. As can be seen, corrosion products distributed across a large area showing the general corrosion characteristics. These results are significant because it is for the first time that an inhibitor has shown the characteristic and capability of mitigating general corroison and also preventing the formation of dominating local corrosion anodes, leading to lower general and local corrosion penetration rates.

Table 1 compares the performance of $La(4OHcin)_3 \cdot 5H_2O$ and [Y (mbp)₃.H₂O] in mitigating waterline corrosion by calculating and comparing total anodic current values. After 1 h of exposure, total anodic current measured from the electrode array exposed to the control solution was 84,430.2 nA while that measured for solutions with La $(4OHcin)_3 \cdot 5H_2O$ and $[Y(mbp)_3 \cdot H_2O]$ were significantly lower (6577.4 nA and 6968.1 nA, respectively). Accordingly, the inhibition efficiencies

are measured to be almost 92% for both inhibitors. Even after 6 h and 12 h of exposure, total anodic currents were slightly increased to 7540 nA and 7977.4 nA, respectively, in the presence of $La(40Hcin)_3 \cdot 5H_2O$, and to 7358.9 nA and 8858.9 nA, respectively, in the presence of $[Y(mbp)_3.H_2O]$. Thus, $La(40Hcin)_3 \cdot 5H_2O$ shows 91% of inhibition efficiency after 6 h and 88% after 12 h while $[Y(mbp)_3.H_2O]$ shows 91% of inhibition efficiency after 6 h and 87% after 12 h of exposure. Therefore, it is clear that these two inhibitors provided significant level of inhibition for waterline corrosion after 1 h, 6 h and 12 h of exposure.

With further increasing the exposure period to 24 h, the inhibition efficiency of La(40Hcin) $_3$ ·5H $_2$ O decreased significantly to 71% and total anodic current increased to 19,056.6 nA. Such decrease in inhibition efficiency and increase in total anodic current correspond with the formation of concentrated anode near waterline as shown in Fig. 2. Inhibition efficiency of the [Y(mbp) $_3$ ·H $_2$ O] also slightly decreased to 86% after 24 h exposure. The inhibition efficiency of La(40Hcin) $_3$ ·5H $_2$ O decreased to 62% after 7 days of exposure and then to 61% after 14 days of exposure, while the inhibition efficiency of [Y(mbp) $_3$ ·H $_2$ O] only decreased gradually to 79% after 7 days and to 76% after 14 days. These changes can be further inferred from Fig. 4 that clearly shows a significant and sudden decrease in inhibition efficiency after 24 h of exposure in the presence of La(40Hcin) $_3$ ·5H $_2$ O while only a gradual decrease in inhibition efficiency after 24 h of exposure in the presence of [Y(mbp) $_3$ ·H $_2$ O].

The decline in the inhibition efficiency of the inhibitors over extended immersion time shown in Fig. 4 and Table 1 could be attributable to a number of factors. For instance, inhibitor could loss efficiency due to the desorption of weakly adsorbed inhibitor species from the steel surface or due to surface film breakdown over time. Peng et al. [44] demonstrated time-dependent loss of the active species of La (40Hcin)₃ from steel surface (more than that of [Y(mbp)₃]). Nam et al. [45] reported hydroxycinnamate-based inhibitor film degradation or breakdown, leading to the formation of porous or thinner films which are less effective at inhibiting corrosion. Nevertheless, under the aggressive waterline corrosion condition, a more likely reason for the observed decline in the inhibition efficiency is competitions between corrosion products such as iron oxides and hydroxides and adsorbed inhibitors or inhibitor films because corrosion products formed on steel surface can physically displace the inhibitors.

However, it should be noted that, total anodic current data in Table 1 only provide an estimation of overall/general corrosion that occurred on the electrode array. Since waterline corrosion is a type of serious localised corrosion, it is important to assess the effects of inhibitors on localised corrosion using data from local areas. Fig. 5 shows corrosion rate maps obtained from the electrode array after 14 days of exposure to the control solution and solutions containing La(4OHcin)₃·5H₂O and [Y (mbp)3.H2O]. As the common scale bar is too large and the local corrosion rate in the presence of [Y(mbp)₃.H₂O] is low, details of Fig. 5c are not clear. Therefore, the scale bar was enlarged and that corrosion rate map was redrawn under a new scale bar as shown in Fig. 5d After 14 days of exposure, significantly different localised corrosion behaviour is clear by comparing corrosion rates from electrode arrays exposed to the control solution, and solutions containing La(4OHcin)₃·5H₂O and [Y (mbp)₃.H₂O]. In solution containing La(4OHcin)₃·5H₂O, major localised corrosion occurred at a concentrated anodes at waterline area and the corrosion rate of that area is around 1.375 mm/y. Bottom area of the probe which exposed to the control solution experienced a corrosion rate around 0.3438 mm/y. However, the highest localised corrosion rate in the presence of [Y(mbp)3.H2O] is 0.1450 mm/y. Those values also prove that $[Y(mbp)_3.H_2O]$ is the most efficient inhibitor for this localised system compared to La(40Hcin)₃·5H₂O. To further verify the differences in localised corrosion behaviour, accumulated corrosion depth maps are produced using in-situ current maps of the type shown in Figs. 1-3 by summing up corrosion losses occurred over the 14 days exposure period, and are presented in Fig. 6.

As shown in Fig. 6, the corrosion depth on the electrode array

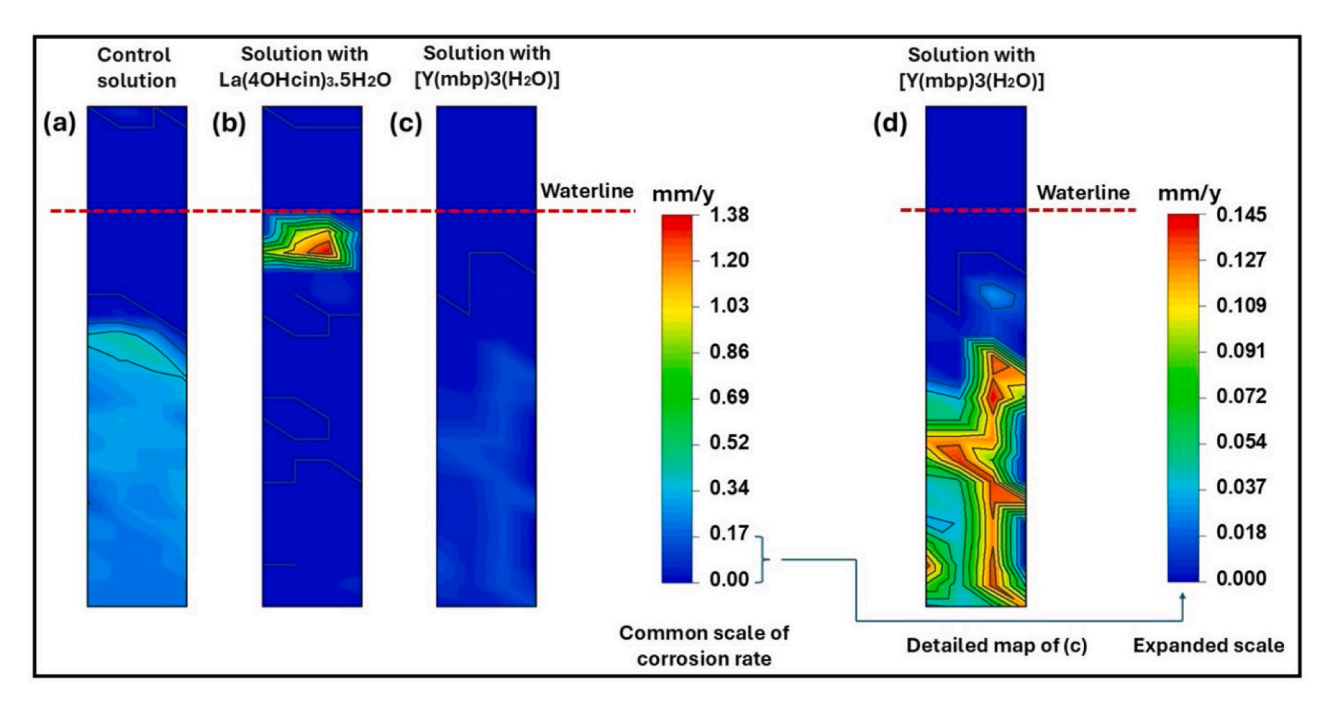


Fig. 5. Corrosion rate maps from the electrode array exposed for 14 days to (a) control solution (3.5 wt% NaCl), (b) solution containing 1 mmol/l La(4OHcin) $_3$ · $5H_2O$ in NaCl, and (c) solution containing 1 mmol/l [Y(mbp) $_3$ · H_2O] in NaCl. Note that a common scale bar used to produce these maps. (d) Detailed corrosion rate map from the electrode array exposed for 14 days to the solution containing 1 mmol/l [Y(mbp) $_3$ · H_2O]. Note that an individual scale bar (expanded scale bar) is used here because current map in (c) doesn't show much details as the range of common scale bar is too large.

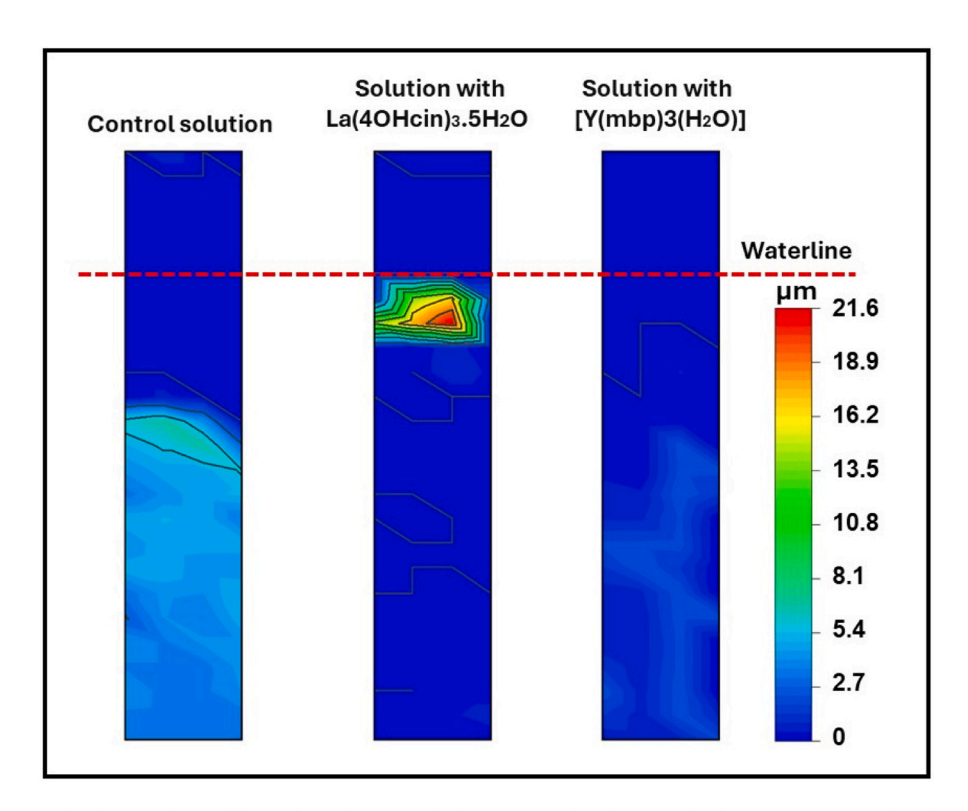


Fig. 6. Accumulated corrosion depth maps obtained from electrode array which was exposed to the control solution (3.5 wt% NaCl), solution containing 1 mmol/l of La(4OHcin) $_3$ · $5H_2O$, and solution containing 1 mmol/l of [Y(mbp) $_3$ · H_2O] for 14 days.

exposed to the control solution is rather generally uniform around the area below the waterline and the average depth value is around 6 μm after 14 days of exposure. However, for the electrode array exposed to the solution containig La(4OHcin)₃·5H₂O, there is a significant localised damage at the waterline and corrosion depth value at those areas is

around 21.6 μm after 14 days of exposure. Clearly, corrosion damage at waterline area was not mitigated by La(4OHcin)₃·5H₂O, while the area below the waterline experienced less corrosion damage in the presence of La(4OHcin)₃·5H₂O compared to that in the control solution. In the presence of [Y(mbp)₃.H₂O],The accumulated corrosion depth is less

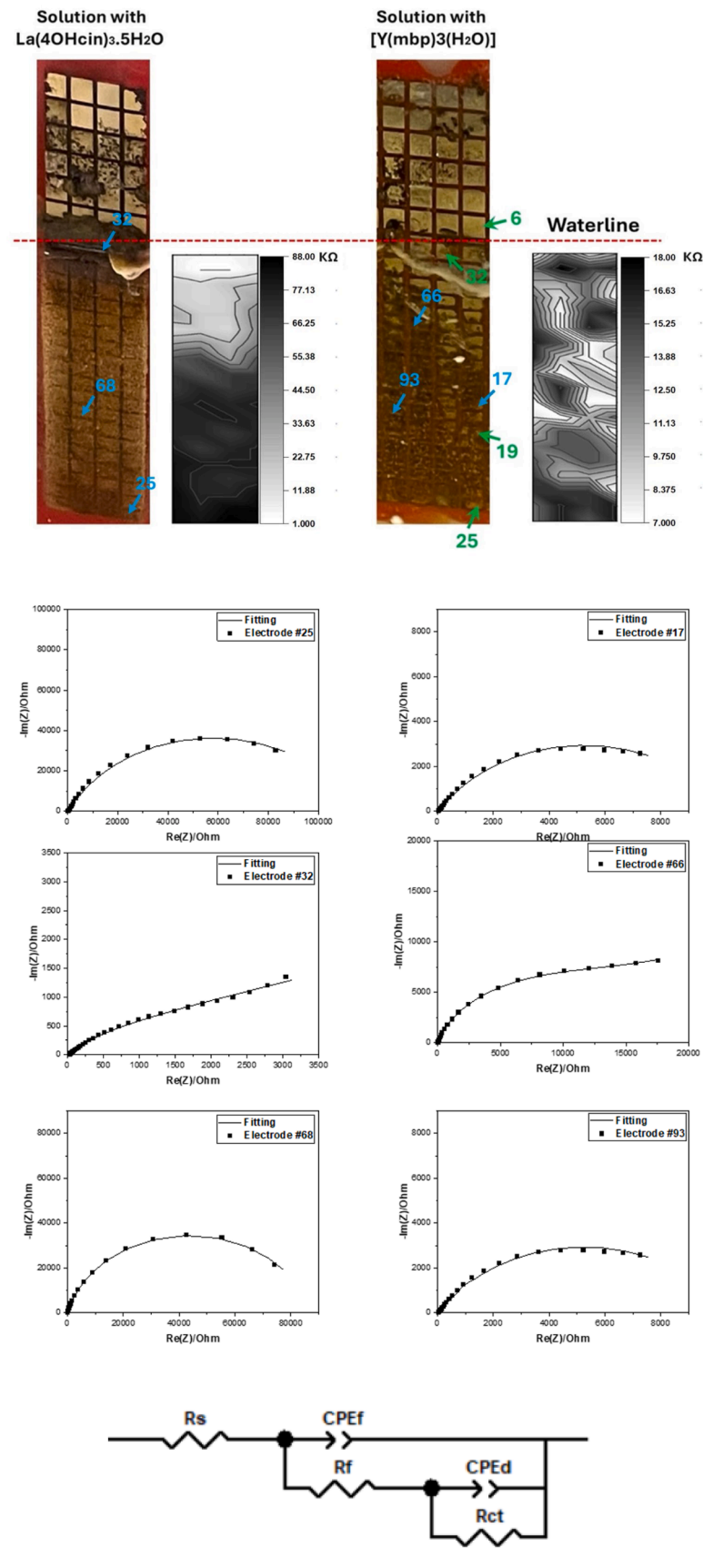
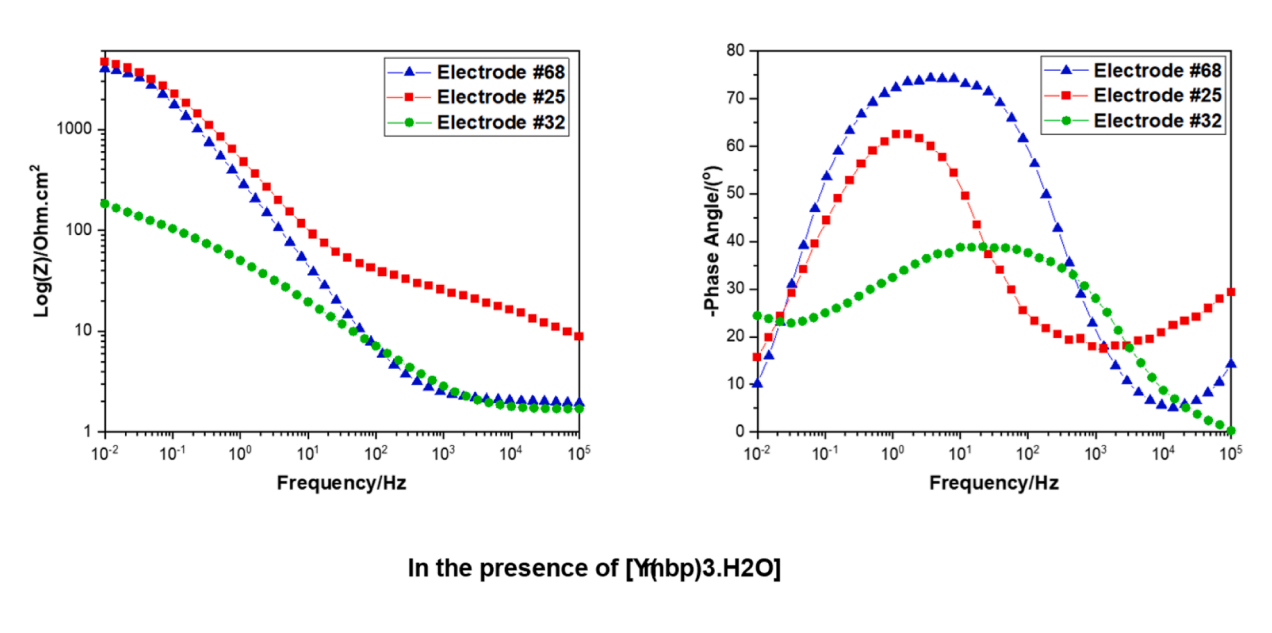


Fig. 7. Local representative Nyquist plots and fittings measured from typical areas of the probe surface; and EIS distribution maps that are drawn using the film resistance values of the fitted graph at each electrode; and the equivelant circuit model used to fit EIS data; and photographs of the electrode array after 14 days of exposure to solutions containing $La(4OHcin)_3 \cdot SH_2O$ and $[Y(mbp)_3 \cdot H_2O]$.

In the presence of La(4OHcin)3.5H2O



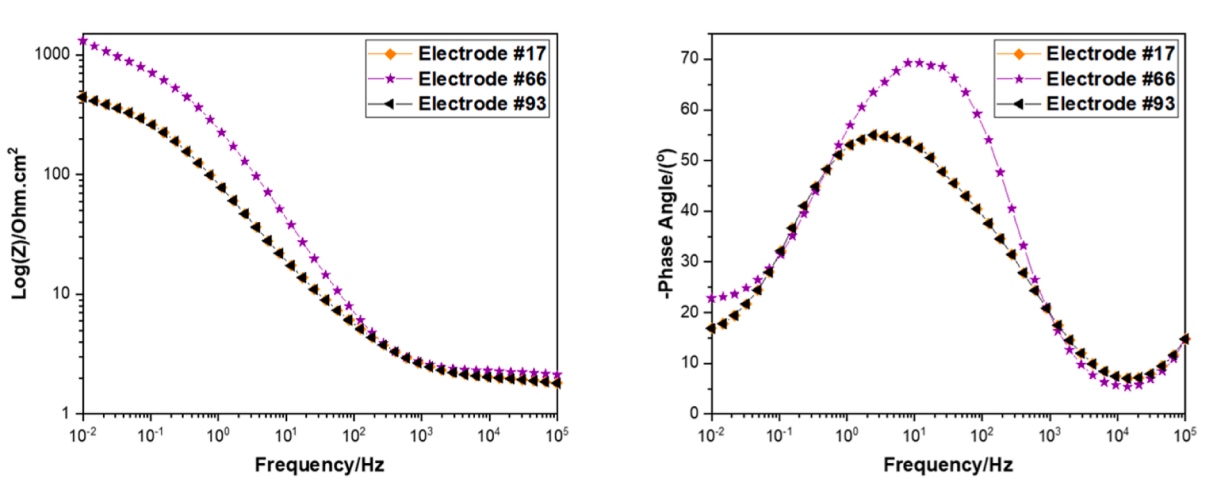


Fig. 8. Impedance modulus and phase angle plots obtained from several locations of the electrode array which was exposed to solution containing 1 mmol/l of La $(40Hcin)_3$ - $5H_2O$, and solution containing 1 mmol/l of $[Y(mbp)_3$ - $H_2O]$ for 14 days.

than 2.70 μm in almost all areas exposed to the solution except a small area at the middle of the elctrode array which shows a corrosion depth around 5.40 μm (as shown in light blue colour). These results clearly show that [Y(mbp)_3.H_2O] has an ability to inhibit localised corrosion at waterline.

3.3. Local electrochemical measurements for understanding localised corrosion inhibition

The next question is why and how these REM inhibitors inhibit waterline corrosion with different behaviour and performances. Although current distribution maps in Figs. 1–3, and corrosion rates and accumulated corrosion depth maps in Figs. 5–6 clearly show different galvanic current distributions over the probe surface in different solutions, resulting in different corrosion patterns, they do not provide an explaination for such differences. It is important to understand mechanisms leading to such differences and to identify features of effective localised corrosion inhibitor. This knowledge would be useful for further discovery and development of new and more effective inhibitors.

In this regard, local EIS measurements were performed at different

individual electrodes under the waterline, as shown in Fig. 7, to explore impedance changes due to inhibitor film formation. Six typical Nyquist plots were taken from representative areas of the probe surfaces after 14 days of exposure to solutions containing La(4OHcin)3.5H2O and [Y (mbp)₃.H₂O]. As shown in Fig. 7, the equivelant circuit model which was used to fit EIS data contains solution resistance (Rs); resistance of the inhibitor film (Rf); CPEf is the constant phase element (CPE) represents the capacitance of the inhibitor film; charge transfer resistance (Rct) and double layer capacitance (CPEd). Fitted EIS parameters are presented as supplementary materials (Supplementary Table 1). Although the Nyquist plots show nonideal impedace behaviour, it is clear that electrodes exposed in La(4OHcin)3.5H2O show large impedance values, while electrodes in [Y(mbp)3.H2O] show both high and low impedance areas. Local Rs values across the whole probe were analised by fitting graphs using the equivelant circuit model shown in Fig. 7. It is clear in the maps that the film formed by La(40Hcin)₃·5H₂O has huge resistance at all the local electrodes except the area just below the waterline where the concentrated corrosion anode was formed and a surface film was not present. However, the film formed by [Y(mbp)₃. H₂O] has both high impedance and low imedpance areas with several

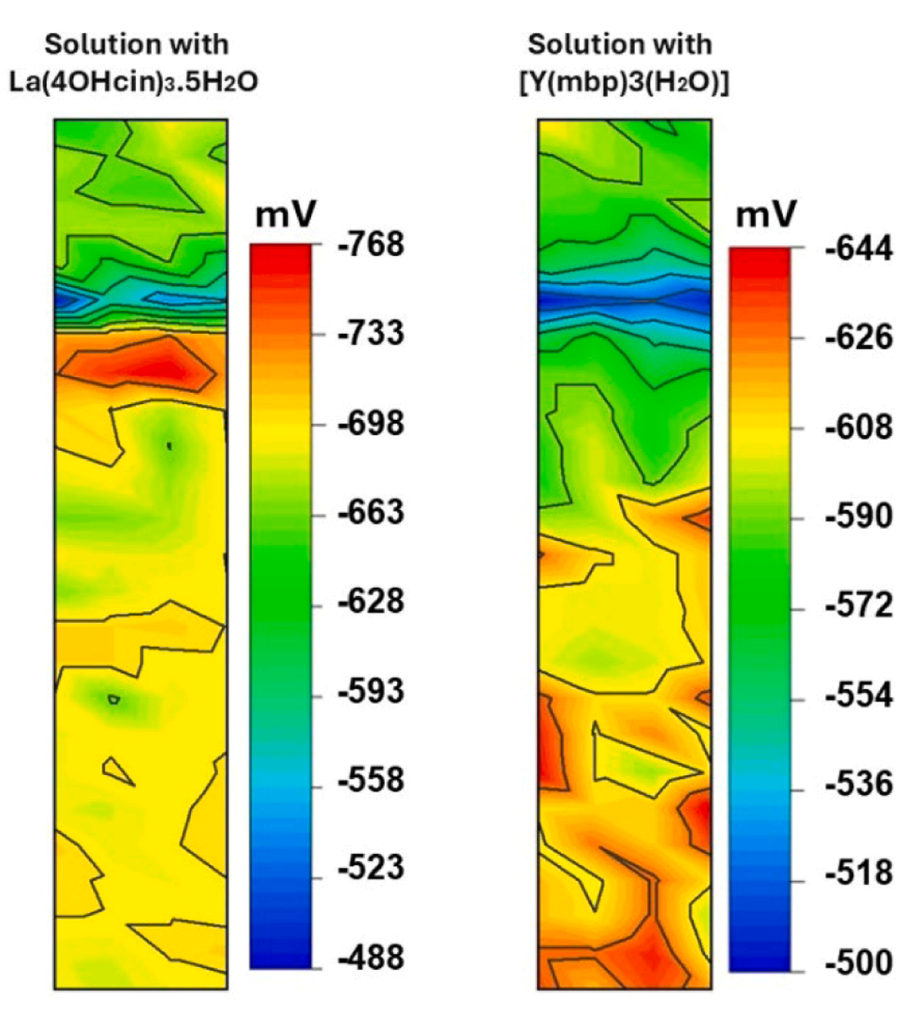


Fig. 9. Local potential distribution maps for the electrod array exposed to the solutions containing La(4OHcin)₃·5H₂O and [Y(mbp)₃·H₂O].

weak points with lower impedance and those points are randomly destributed across the electrode array surface. These results suggest that the film formed by $[Y(mbp)_3.H_2O]$ has a special feature: it has a nonuniform structure with some low impedance cavities in the film that allow the formation of random anodic sites. The existence of these anodes avoided the formation of dominating anodes, and therefore prevent major localised corrosion. This characteristic is similar to an inhibitor reported in a previous study that shows Resorcinarene acid inhibited localised CO_2 corrosion of steel which exposed to CO_2 saturated brine solution by forming randomly distributed minor anodes [43].

Fig. 8 shows the impedance modulus and phase angle plots obtained from the several locations of the electrode array after 14 days of exposure to La(4OHcin)₃·5H₂O and [Y(mbp)₃.H₂O]. In the presence of La (40Hcin)₃·5H₂O, the impedance of electrode #32 at low frequency range shows significant lower value compared to electrode #68 and #25. This could be an indication of higher corrosion at that location which agrees with the corrosion rate and corrosion depth maps (Figs. 5 and 6). Further, in the presence of [Y(mbp)₃,H₂O], the impedance shown by electrode #17 and #93 at lower frequency are lower than the impedance shown by electrode #66. Therefore, the corrosion rates at electrodes #17 and #93 are higher than the corrosion rate at electrode #66. Impedance values at each electrode gradually decrease and become relatively stable at the high frequency range. Phase angle of each local electrode increased at low frequency range, reached the highest value at middle frequency range and decreased at high frequency range. At highest frequency range $(10^4 - 10^5 \text{ Hz})$, phase angle shows slight increase at all electrodes except electrode #32.

Morphology of the film formed in the solution containing La

 $(40 Hcin)_3 \cdot 5H_2O$ looks similar to the passive film formed in an alkaline solution (Evans solution, pH \sim 11) reported previously [2,46]. In Evans solution, localised corrosion occurs at the area where passivity breakdown occurs (at the waterline) while other areas covered by the passive layer behave as active cathodic areas, leading to serious localised corrosion penetration [10,46]. Similarly, La(40Hcin) $_3 \cdot 5H_2O$ converts the bottom area of the electrode array into cathodes with low current values (see Fig. 2) and therefore other anodes are unable to co-exist except the dominating anodes that terminates all other anodes, a phenomenon similar to those reported in reference [9].

One of main features of significant localised corrosion such as in Evans solution is large potential difference between anodic and cathodic sites. According to the literature, the potential difference between major anodes and major cathodes in Evans solution can be up to 600 mV [9, 46]. To check the potential differences between anodes and cathodes in the presence of each inhibitor, local potential distribution maps were measured as shown in Fig. 9. The potential difference between major anode and cathode in the presence of La(40Hcin) $_3$ ·5H $_2$ O is 280 mV, whereas [Y(mbp) $_3$.H $_2$ O] shows 144 mV potential difference. So, the potential difference in the presence of La(40Hcin) $_3$ ·5H $_2$ O is about two times higher than the potential difference in the presence of [Y(mbp) $_3$. H $_2$ O]. These results explain why the galvanic activities were so strong in the La(40Hcin) $_3$ ·5H $_2$ O containg solution, leading to very high localised corrosion rates shown in Fig. 5 and significant local corrosion damages shown in Fig. 6.

Further, local polarisation measurements are conducted to evaluate local electrochemistry with the presence of these inhibitors and to identify differences in the behaviour of REM carboxylates in inhibiting

Electrochimica Acta 528 (2025) 146307

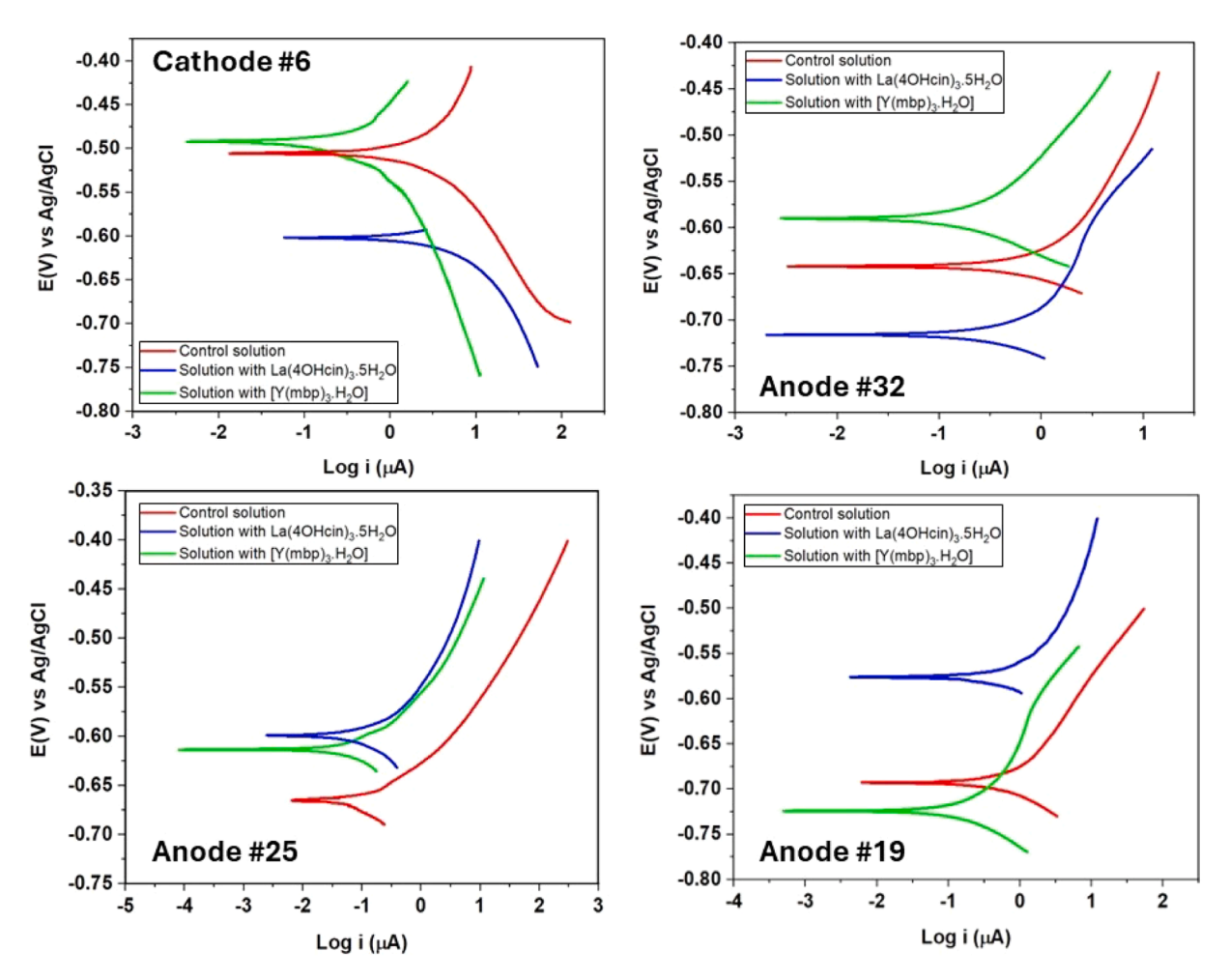
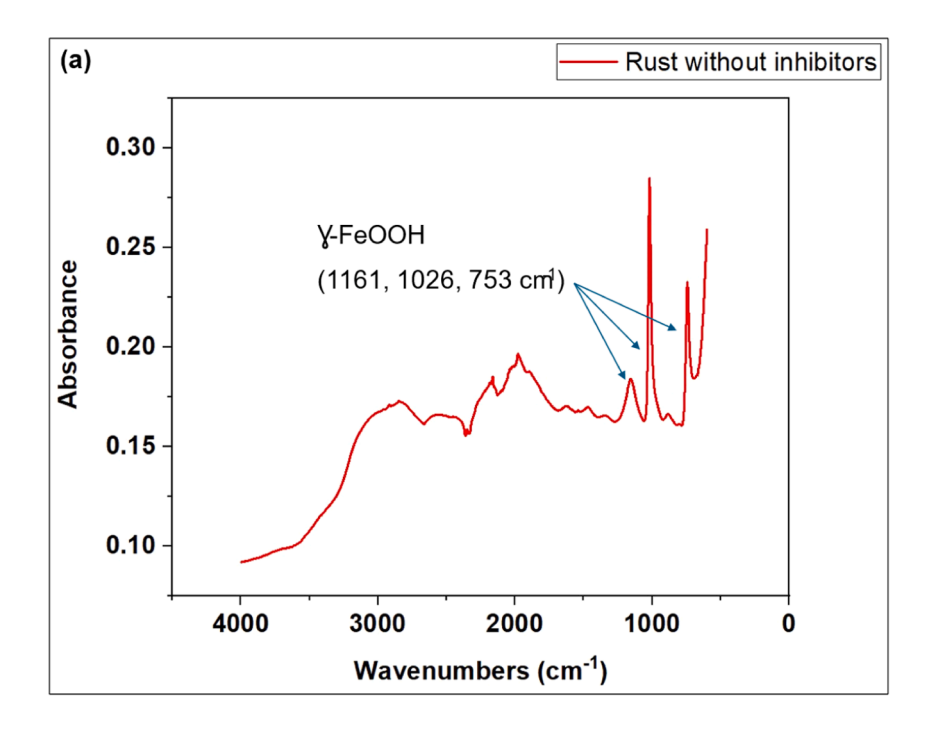


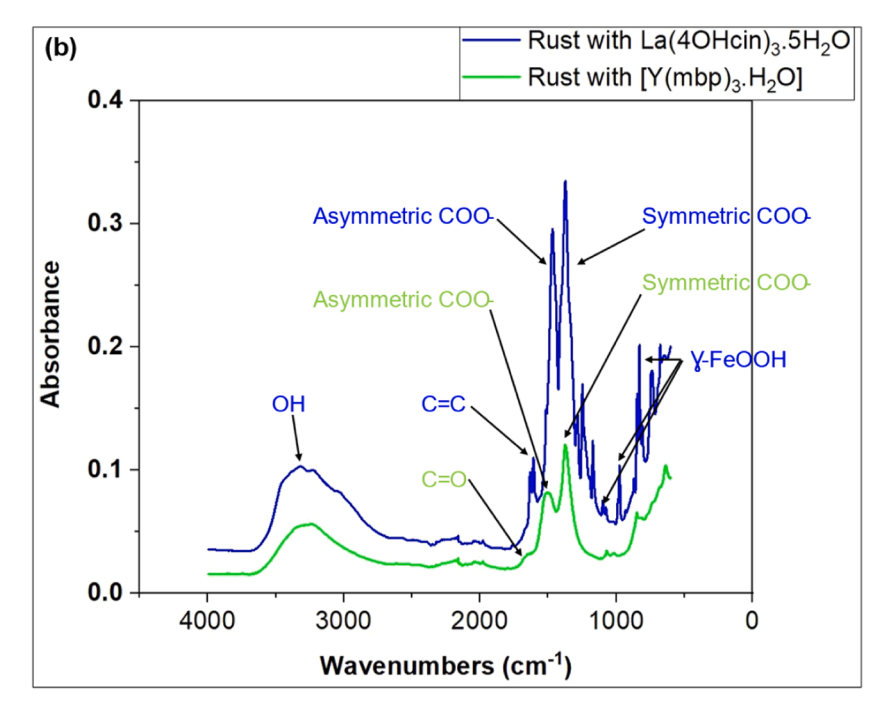
Fig. 10. Local polarisation curves on cathode #6, anode #32 where the concentrated anode located in the presence of $La(40Hcin)_3 \cdot 5H_2O$, anode #25 where La $(40Hcin)_3 \cdot 5H_2O$ forms a film with large resistance, and anode #19 where $[Y(mbp)_3 \cdot H_2O]$ forms a weak point with relatively low resistance on its' protective layer. For the position of the electrodes on the electrode array, please refer to the green numbers in Fig. 7.

waterline corrosion that could be related to the formation of surface films with different characteristics. As shown in Fig. 10 for cathode #6, cathodic kinetics in the presence of an inhibitor are lower compared to those in the control solution. Note that the location of the electrodes where local polarisation measurements are carried out previously indicated by green arrows in Fig. 7. Lowest cathodic kinetics are shown in the presence of [Y(mbp)₃.H₂O]. So, it is clear that both of the inhibitors can reduce cathodic kinetics at cathodes. For anode #32, the anodic kinetics are a bit higher in the presence of La(4OHcin)3.5H2O than that of the control solution. This is the location where the concentrated anode is formed by La(4OHcin)3.5H2O. So, it is clear that La (4OHcin)₃·5H₂O is unable to mitigate corrosion at this local area. However, anodic kinatics are lower in the presence of [Y(mbp)₃.H₂O] compared to the control solution indicating that this inhibitor mitigates the corrosion at this location. For anode #25, anodic kinetics are redused in the presence of both inhibitors compared to the control solution. At this location, film resistance is large in the presence of each inhibitor. For anode #19, anodic kinatics in the presence of La (4OHcin)₃·5H₂O is the lowest. Anodic kinetics in the presence of [Y (mbp)₃.H₂O] at this location is lower compared to the control solution. However, that is not a large reduction compared to anode #25. Please note that [Y(mbp)₃.H₂O] formed a weak point with lower film resistance at this location (anode #19). Extracted Tafel extrapolation data, including I_{corr} , E_{corr} , B_{a} , and B_{c} are pesented as supplementary materials (Supplementary Table 2).

The intense anodic sites detected in the galvanic current maps when

La(4OHcin)₃·5H₂O is used as inhibitor are most likely due to localised breakdown of corrosion inhibitor films at local anodic sites where significant amount of corrosion products such as iron oxides and hydroxides formed under the aggressive waterline corrosion condition. Corrosion products formed on steel surface can physically displace the adsorbed inhibitors or inhibitor films. Another factor is the local acidification at these anodic sites. Lanthanum and ferric ions can hydrolyse in aqueous solution (La³⁺ + 3H₂O \rightarrow La(OH)₃ + 3H⁺; Fe³⁺ + 3H₂O \rightarrow Fe (OH)₃ + 3H^{*}), generating localised acidity and creating an active anodic corrosion environment that promotes Fe dissolution. This is consistent with the results reported by Seter et al. [47] who showed that La³⁺ hydrolysis enhances local acidification, which could explain the breakdown of passive films and the intense anodic activity at anodic areas. Furthermore, the pH-dependent speciation of La(4OHcin)₃ has been shown to influence its inhibition mechanism. At low pH, the complex dissociates into [LaCl4]- and cinnamate, leading to mixed or predominantly cathodic inhibition, while at neutral to alkaline pH, more complex species like $[LaL_4]^-$ become prevalent, which are associated with anodic inhibition [47]. In contrast, the [Y(mbp)₃·H₂O] complex appears to form a more stable and continuous surface film, likely facilitated by stronger interactions between the methoxybenzoyl ligands and the steel oxide/hydroxide surface. The mbp ligands lack redox-active phenolic groups, reducing the likelihood of film disruption. The result is a more uniform inhibition effect across the steel surface as reflected in both the galvanic current maps, local EIS, and local polarisation measurement, although the film has lower impedance and has 'weak' areas allowing





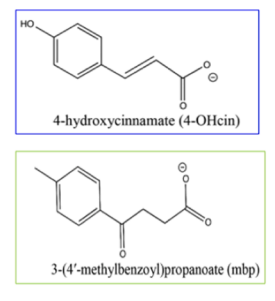


Fig. 11. FTIR spectrum obtained from (a) rust without any inhibitor and (b) the deposit in the presence of La(4OHcin)₃· $5H_2O$ and in the presence of [Y(mbp)₃. H_2O] in blue and green colour, respectively.

minor anodes to form.

To understand the composition of deposits formed by each inibitor, FTIR was conducted. Fig. 11a shows the FTIR spectrum obtained from rust without any inhibitor. It clearly shows peaks corresponds to $\gamma\text{-FeOOH}$. Fig. 11b shows the spectra obtained from the deposit in the presence of La(4OHcin)_3·5H_2O in blue colour and in the presence of [Y (mbp)_3.H_2O] in green colour. It is an evidence for the formation of protective layers by these two inhibitors. These protective layers should be the reason for decreasing corrosion rates compared to control solution. Table 2 summarises the analysis of the each peak in three spectra.

To obtain these results, whole deposit on the probe was removed and FTIR was conducted using those powders.

According to Table 2, rust formed on the electrode array surface exposed to the control solution (without any inhibitor) shows peaks at 742, 879, 1020 cm^{-1} corresponding to different types of iron hydroxide and a broad peak at approximately 3000 cm^{-1} which is corresponding to OH in water and metal oxyhydroxide [48]. The deposit formed in the solution containing La(4OHcin)₃·5H₂O also shows peaks corresponding to iron hydroxides. Further, three peaks are observed which are corresponding to COO and C = C, displaying strong absorption bands at 1375,

Table 2Analysis of each peak of the FTIR spectra obtained from three different deposits.

	Rust without inhibitor / cm ⁻¹	Rust with La (40Hcin) ₃ ·5H ₂ O / cm ⁻¹	Rust with [Y (mbp) ₃ .H ₂ O] / cm ⁻¹
Feroxyhyte		677	640
(γ'-FeOOH)			
Lepidocrocite	742	736	
(γ-FeOOH)		000	
Feroxyhyte		829	
Feroxyhyte	879	869	850
Lepidocrocite	1020	995	
Feroxyhyte		1099	1070
Lepidocrocite	1159	1172	
COO symmetrical		1375	1371
COO asymmetrical		1470	1500
C = C		1618	
C = O			1654
OH in water	2844	3321	3288

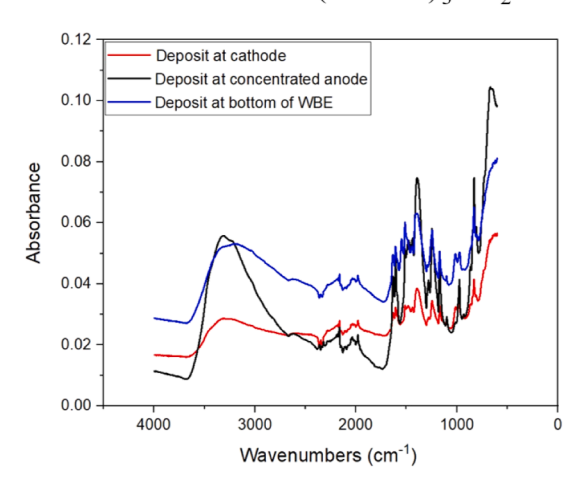
1470 and 1631 cm⁻¹. The deposit formed in the solution containing [Y (mbp)₃.H₂O] shows peaks corresponding to iron hydroxide, however those bands are remarkebly weak compared to rust sample without any inhibitor and rust sample with La(4OHcin)3.5H2O which is another evidance for low corrosion in the presence of [Y(mbp)3.H2O]. Further, bands correspond to COO and C = O occur at 1371, 1500 and 1654 cm⁻¹ respectively in the presence of [Y(mbp)3.H2O]. So, in summary, all three samples show peaks corresponding to iron hydroxide and OH. In the presence of inhibitors, there are peaks corresponding to COO. Main difference in spectra of two inhibitors is La(4OHcin)3.5H2O shows a peak corresponding to C = C while [Y(mbp)₃.H₂O] shows a peak corresponding to C = O. The shift of the C = O of the [Y(mbp)₃.H₂O] from that of the neat compound (wavenumber is 1678 cm⁻¹ [41]) strongly suggests an interaction of the carbonyl group with Fe in the film. Similarly, these results suggest that there is an interaction between C = Cof La(4OHcin)₃·5H₂O with Fe (wavenumber corresponds to C = C of neat compound is 1631 cm⁻¹ [48]). Overall, IR suggests that these two inhbitors form Fe/carboxylate/Y (by [Y(mbp)3.H2O]) and Fe/carboxvlate/La (by La(40Hcin)3:5H2O) bimetallic film to inhibit corrosion which agrees with literature [28]. To obtain site-specific information, FTIR was performed on the deposits acquired from local anodic and cathodic sites of the probe which is exposed to each inhibitor as shown in Fig. 12.

As shown in Fig. 12, spectra obtained from the deposits on cathodic

sites in the presence of each inhibitor show significant differences compared to that from anodic sites. First difference is the peaks corresponding to corrosion products (rust) are weak compared to those from anodic sites. This is an indication that rust is deposited on anodic sites only. Further, in the spectra from cathodic sites, there is a broad band at around 3000 cm⁻¹ which attributes to OH vibration. This could be due to La(OH)₃ in the presence of La(4OHcin)₃·5H₂O and Y(OH)₃ in the presence of [Y(mbp)₃,H₂O]. These REM hydroxide precipitate can act as a physical barrier to oxygen penetration at cathodic sites. This may be the reason for reduction in cathodic kinetics in the presence of each inhibitor compared to control solution as shown in local polarisation curves in Fig. 3. This agrees with the literature. According to a mechanism proposed by Forsyth et al., a protective film is formed over the cathodic site by precipitation of REM ions as REM hydroxide and this was supported by surface analytical technics such as SEM-EDS and ATR-FTIR [28]. Jichavo et al. also showed that REM inhibitors mitigate corrosion by hydroxide precipitation due to a pH increase at local cathodic areas where the oxygen reduction reaction occurs [35]. There are also sharp peaks at about 3000 cm⁻¹ in the spectra acquired from anodic sites but these peaks can be attributed to OH in water (as anodic sites are in contact with water) and hydroxyl groups from iron oxyhydroxide compound.

If we consider the FTIR spectra obtained from anodic sites in the presence of each inhibitor as shown in Fig. 12, there are sharp peaks correspond to COO vibrations around 1370 cm⁻¹ in the presence of each inhibitor. Further, La(4OHcin)₃·5H₂O shows a peak corresponding to C = C while [Y(mbp)₃.H₂O] shows a peak corresponding to C = O in the specra obtained from anodic sites and these are strong peaks compared to those in the spectra obtained from cathodic sites. This indicates that each inhibitor involves in the film formation on the anodic sites. Further, the shifts of COO (wavenumbers correspond to symmetric and asymetric COO of neat compound are 1399 and 1557 cm⁻¹ respectively [41]) and C = O from the neat compound suggest interactions of COO and C = Owith Fe in the film in the presence of [Y(mbp)₃.H₂O]. Similarly, there can be interactions of COO (wavenumbers correspond to symmetric and asymetric COO of neat compound are 1392 and 1509 cm⁻¹ respectively [48]) and C = C with Fe in the film in the presence of La (4OHcin)₃·5H₂O. Based on comparisons of corroded steel surfaces to model compounds, speciation studies and surface analytical techniques such as SEM-EDS and ATR-FTIR, Forsyth et al. [28] proposed that REM carboxylate compounds bind to a steel surface by forming a bimetallic Fe-carboxylate-REM complex film over the anodic sites and hence reduce the iron dissolution (Fe_(s) \rightarrow Fe²⁺_(aq) + 2e). According to the studies done by Somers et al., Peng et al. and Seter et al., it was believed that the

Solution withLa(4OHcin)₃.5H₂O



Solution with $[Y(mbp)_3.H_2O]$

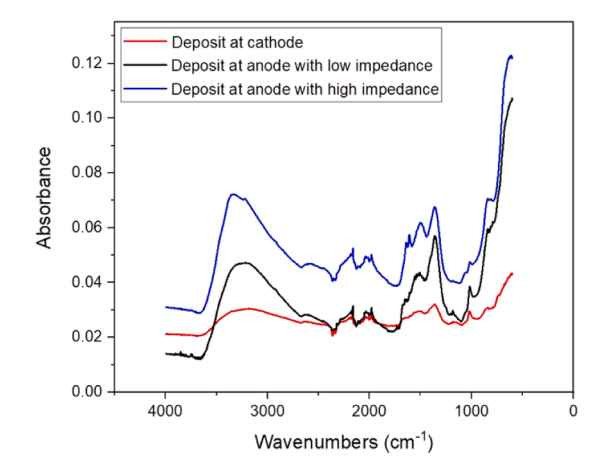


Fig. 12. FTIR spectrum obtained on the deposit acquired from local anodic and cathodic sites of the electrode array which exposed to solutions containing (a) La (40Hcin)₃·5H₂O and (b) [Y(mbp)₃·H₂O].

REM plays a major role in the speciation of REM carboxylate complexes in the solution and affects the formation of an effective and stable bimetallic surface film [42,49,50].

According to the local EIS distribution maps shown in Fig. 7, it is clear that the protective film formed by these two inhibitors are different which in turn lead to difference in inhibition behaviour and performance by these two inhibitors. In the presence of La(40Hcin)₃·5H₂O, a protective film with high impedance is formed over the bottom part of the electrode array while a film with low impedance is formed at the concentrated anode near the waterline according to EIS destribution map. However, there is not any significant difference of the FTIR spectra obtained from these two locations as the composition of the films at these two locations are similar as shown in Fig. 12. Furthermore, [Y (mbp)₃.H₂O] forms a protective layer with some weak points with low impedance while the impedance of the film at other areas are high according to EIS destribution map shown in Fig. 7. However, the FTIR spectra obtained from these two locations do not show significant difference as shown in Fig. 12, indicating that the composition of the film at these two locations are similar. Further investigations are required to reveal the reasons caused for the deference in protective film at different locations formed by each inhibitor because that is directly related to the difference in inhibition performance of these two REM carboxylate

In summary, the most significant and clear difference between these two inhibitors is that the film formed in $[Y(mbp)_3.H_2O]$ is non-homogenuos as there are weak points with low impedance in this film which allow to form minor anodes over the surface and that is the reason for $[Y(mbp)_3.H_2O]$ to be an efficient inhibitor for localised corrosion. This suggests that effective localised corrosion inhibitor should be sourced from chemicals that possess the ability not only to reduce the overall corrosion currents, but also the ability to avoid the formation of major local anodes by generating large number of minor anodes randomly distributing over the steel surface, leading to insignificant general corrosion. Local impedance maps such as those shown in Fig. 7 could be used as a tool to discover new and effective localised corrosion inhibitors.

This study provides direct evidences that effective and environmentally friendly localised corrosion inhibitor could be found by exploring and understanding the local electrochemical behaviour of corrosion inhibitors using complementary in-situ monitoring of galvanic currents and site-specific localised polarisation and EIS measurements. It also shows that two structurally distinct rare-earth organic complexes, La(4OHcin)₃·5H₂O and [Y(mbp)₃·H₂O], behave very differently in localised corrosion inhibition although both of them perform well in inhibiting general corrosion. This study has clear implications for realworld corrosion control strategies, particularly in scenarios where localised corroison is the dominant degradation problem such as steel structures in marine atmospheres or cooling water systems, in pipelines, tanks, offshore platforms. In this context, the [Y(mbp)₃·H₂O] complex demonstrates good long-term inhibition performance, suggesting its potential for use in coating additives, in corrosion-inhibiting surface treatment solutions, or in circulating water systems for corrosion control. Additionally, it shows that the methodology employed here can serve as a screening tool for discovering more effective and durable corrosion inhibition technologies.

4. Conclusions

This study investigated the effectiveness of two different rare earth metal (REM) inhibitors in mitigating waterline corrosion through local electrochemical measurement using an electrode array. The impact of the two inhibitors on corrosion behaviour was assessed by analysing time-lapse local current distributions at the waterline over an extended period of time. La(4OHcin)₃·5H₂O which effectively inhibit general corrosion was found to exacerbate localised corrosion at the waterline by generating pronounced anodic sites with high current densities. This

effect not only intensified corrosion but also led to highly uneven metal degradation, making it unsuitable as a corrosion mitigation strategy. In contrast, $[Y(mbp)_3.H_2O]$ demonstrated effective localised corrosion mitigation by promoting a more general corrosion pattern across the metal surface. $[Y(mbp)_3.H_2O]$ was able to suppress the formation of discrete and dominating anodic sites, thereby limiting localised damage and enhancing the overall inhibition efficiency. The most significant and clear difference between these two inhibitors is that the film formed in $[Y(mbp)_3.H_2O]$ is non-homogenuos as there are weak points with low impedance in this film which allow to form minor anodes over the surface and that is the reason for $[Y(mbp)_3.H_2O]$ to be an efficient inhibitor for localised corrosion. This work also demonstrates a new approach to discovering localised corrosion inhibitors through local electrochemical measurements using electrode arrays.

CRediT authorship contribution statement

Medhani Pathirana: Writing – review & editing, Writing – original draft, Visualization, Validation, Methodology, Investigation, Formal analysis, Data curation, Conceptualization. Majid Laleh: Writing – review & editing, Visualization, Validation, Supervision, Methodology, Investigation, Formal analysis, Data curation. Anthony Somers: Writing – review & editing, Validation, Supervision, Methodology, Investigation, Formal analysis, Data curation. Bruce Hinton: Writing – review & editing, Supervision, Investigation, Formal analysis. Glenb. Deacon: Writing – review & editing, Funding acquisition, Formal analysis, Conceptualization. PeterC. Junk: Writing – review & editing, Formal analysis, Conceptualization. MikeYongjun Tan: Writing – review & editing, Visualization, Validation, Supervision, Resources, Project administration, Methodology, Funding acquisition, Formal analysis, Data curation, Conceptualization.

Declaration of competing interest

The authors declare that they have no known competing financial interests or personal relationships that could have appeared to influence the work reported in this paper.

Acknowledgments

Financial support from Australian Research Council funding for ARC Discovery project ID: DP200100568 is gratefully acknowledged.

Supplementary materials

Supplementary material associated with this article can be found, in the online version, at doi:10.1016/j.electacta.2025.146307.

Data availability

The raw/processed data required to reproduce these findings cannot be shared at this time as the data also forms part of an ongoing study.

References

- M. Laleh, Y. Huo, M.B. Kannan, R.B. Petersen, R.E. Melchers, M.Y.J. Tan, Probing and monitoring multiple forms of localised corrosion occurring concurrently on pipeline steels in marine environments. Corros. Sci. 214 (2024) 112453.
- [2] M. Laleh, Y. Huo, R.E. Melchers, M.Y.J. Tan, Electrode array probe designed for visualising and monitoring multiple localised corrosion processes and mechanisms simultaneously occurring on marine structures, NPJ Mater. Degradat. 7 (2023) 68.
- [3] B. Piri, R. Amini, E. Asadinia, S. Vardak, R. Mehdilouee, A. Mojarrad, Investigation of failure mechanisms and remaining life prediction of firewater pipelines used in industrial applications, Eng. Fail. Anal. 124 (2021) 105301.
- [4] J.A. Beavers, N. Sridhar, K.D. Boomer, Corrosion management of the Hanford highlevel nuclear waste tanks, JOM 66 (3) (2014) 491–502.

- [5] X. Li, F. Gui, H. Cong, C. Brossia, G. Frankel, Examination of mechanisms for liquidair-interface corrosion of steel in high level radioactive waste simulants, J. Electrochem. Soc. 160 (11) (2013) C521.
- [6] R. Ray, J. Lee, B. Little, Factors contributing to corrosion of steel pilings in Duluth-Superior Harbor, Corrosion 65 (11) (2009) 707.
- [7] M. Peterson, L.J. WALDRON, Investigation of mild steel corrosion rate in San Diego harbor, Corrosion 17 (4) (1961) 188t–190t.
- [8] J. De Gruyter, S. Mertens, E. Temmerman, Corrosion due to differential aeration reconsidered, J. Electroanal. Chem. 506 (1) (2001) 61–63.
- [9] Y. Tan, Monitoring localized corrosion processes and estimating localized corrosion rates using a wire-beam electrode, Corrosion 54 (5) (1998) 403–413.
- [10] M. Pathirana, M. Laleh, A. Somers, B. Hinton, M.Y. Tan, The critical effect of rust layers on localised corrosion of steel exposed to waterline environments, Corros. Sci. 221 (2023) 111333.
- [11] M. Laleh, M. Pathirana, M.Y. Tan, Site-specific local polarisation curve measurements for probing localised corrosion and inhibition, Corros. Sci. 214 (2023) 111019.
- [12] I. Rosenfeld, I. Marshakov, Mechanism of crevice corrosion, Corrosion 20 (4) (1964) 115t-125t.
- [13] G. Singh, Corrosion inhibitors, Corros. Rev. 27 (2009) 367-416.
- [14] K. Rasmussen, A. Wright, M.J. Schofield, H. Lund, Investigation of a corrosion failure in an offshore gas compression system: The role of H2S Scavenger and organic acids, NACE International, 2004. CORROSION 2004.
- [15] K. Rajagopal, R. Lacerda, I. Slobodcicov, E. Campagnolo, Modeling and simulation of hydrogen sulfide removal from petroleum production lines by chemical scavengers, Chem. Eng. Commun. 196 (2009) 1237–1248.
- [16] M. Davies, P. Scott, Oilfield Water Technology, NACE International Houston, TX2006.
- [17] J. Fink, Oil Field Chemicals, Elsevier, 2003.
- [18] S.A.M. Refaey et al. rApplied Surface Science 158 2000 190-196.
- [19] S.A.M. Refaey, manuscript submitted for publication in Appl, Surf. Sci. (1999).
- [20] H.P. Leckie, H.H. Uhlig, Environmental factors affecting the critical potential for pitting in 18 –8 stainless steel, J. Electrochem. Soc. 113 (1966) 1262–1267.
- [21] I.L. Rozenfeld, J.S. Danilov, Electrochemical aspects of pitting corrosion, Corros. Sci. 7 (1967) 129–142.
- [22] R.C. Newman, T. Shahrabi, The effect of alloyed nitrogen or dissolved nitrate ions on the anodic behaviour of austenitic stainless steel in hydrochloric acid, Corros. Sci. 27 (1987) 827–838.
- [23] E.A. Abd El Meguid, A.A. Abd El Latif, Electrochemical and SEM study on type 254 SMO stainless steel in chloride solutions, Corros Sci. 46 (2004) 2431–2444.
- [24] C.S. Brossia, R.G. Kelly, Infl uence of alloy sulfur content and bulk electrolyte composition on crevice corrosion initiation of austenitic stainless steel, Corrosion 54 (1998) 145–154.
- [25] B.R.W. Hinton, P.N. Trathen, L. Wilson, The inhibition of mild steel corrosion in tap water by cerous chloride, in: 28th Annual Conference of Australasian Corrosion Association, Australasian Corrosion Association, Perth. Australia, 1988.
- [26] B.R.W. Hinton, New Approaches to Corrosion Inhibition with Rare Earth Metal Salts, 89, NACE, New Orleans, 1989. CorrosionPaper No. 170.
- [27] A.D. Mercer, The properties of carboxylates as corrosion inhibitors, in: Proc 5th European Symposium on Corrosion Inhibitors, Ferrara, Italy, 1980, pp. 563–581.
- [28] M. Forsyth, M. Seter, B. Hinton, G. Deacon, P. Junk, New 'green' corrosion inhibitors based on rare earth compounds, Aust. J. Chem. 64 (2011) 812–819.
- [29] F.J. Blin, S. Leary, K.E. Wilson, M. Forsyth, Evaluation of the Corrosion Mitigation Potential of Some New Rare Earth Metal Based Compounds On Steel, 02, Australasian Corrosion Association, Adelaide, 2002, p. 79. CorrosionPaper.
- [30] F.J. Blin, S. Leary, K.E. Wilson, The inhibition of corrosion on mild steel with rare earth cinnamate compounds. Corrosion Control and NDT, Australasian Corrosion Association, Melbourne, 2003, p. 80, 2003.
- [31] F. Blin, P. Koutsoukos, P. Klepetsianis, The corrosion inhibition mechanism of new rare earth cinnamate compounds – Electrochemical studies, Electrochim Acta 52 (21) (2007) 6212–6220.

- [32] M. Behrouzvaziri, The Effect of Concentration and Structure on La and Ce based inhibitors on the Corrosion Rate of Mild Steel in Chloride Solution, Monash University MEngSc Thesis, Melbourne, 2009.
- [33] M. Behrouzvaziri, B.R.W. Hinton, M. Forsyth, The effect of concentration and structure on La and Ce based inhibitors on the corrosion rate of mild steel in chloride solution, Corros. Prevent. (2008). Nov 2008.
- [34] F. Blin, S.G. Leary, K. Wilson, Corrosion mitigation of mild steel by new rare earth cinnamate compounds, J. Appl. Electrochem. (2004) 591–599.
- [35] J. Li, B. Hurley, R. Buchheit, Microelectrochemical characterization of the effect of rare earth inhibitors on the localized corrosion of AA2024-T3, J. Electrochem. Soc. 162 (10) (2015) C563–C571, https://doi.org/10.1149/2.0791510jes.
- [36] G.B. Deacon, P.C. Junk, W.W. Lee, M. Forsyth, J. Wang, Rare earth 3-(4'-hydroxyphenyl) propionate complexes, New J. Chem. 39 (2015) 7688–7695.
- [37] C.N. de Bruin-Dickason, G.B. Deacon, C.M. Forsyth, S. Hanf, O.B. Heilmann, B.R. W. Hinton, P.C. Junk, A.E. Somers, Y.Q. Tan, D.R. Turner, Synthesis and structures of rare earth 3-(4'-methylbenzoyl)-propanoate complexes-new corrosion inhibitors, Aust. J. Chem. 70 (2017) 478–484.
- [38] M. Frey, S.G. Harris, J.M. Holmes, D.A. Nation, S. Parsons, P.A. Tasker, S.J. Teat, R. E. Winpenny, Modeling surface engineering: use of polymetallic iron cages and computer graphics to understand the mode of action of a corrosion inhibitor, Angew. Chem. Int. Ed. 37 (1998) 3245–3248.
- [39] M. Frey, S.G. Harris, J.M. Holmes, D.A. Nation, S. Parsons, P.A. Tasker, R. E. Winpenny, Elucidating the mode of action of a corrosion inhibitor for iron, Chem. Eur. J. 6 (2000) 1407–1415.
- [40] F. Blin, S. Leary, K. Wilson, G. Deacon, P. Junk, M. Forsyth, Corrosion mitigation of mild steel by new rare earth cinnamate compounds, J. Appl. Electrochem. 34 (2004) 591–599.
- [41] A.E. Somers, et al., Advances in the development of rare earth metal and carboxylate compounds as corrosion inhibitors for steel, Corros. Eng. Sci. Technol. 55 (4) (2020) 311–321, https://doi.org/10.1080/1478422x.2020.1754600.
- [42] Y. Peng, et al., A study of rare-earth 3-(4-methylbenzoyl)-propanoate compounds as corrosion inhibitors for AS1020 mild steel in NaCl solutions, Corros Sci. 145 (2018) 199–211, https://doi.org/10.1016/j.corsci.2018.09.022.
- [43] Y. Tan, M. Mocerino, T. Paterson, Organic molecules showing the characteristics of localised corrosion aggravation and inhibition, Corros Sci. 53 (5) (2011) 2041–2045. https://doi.org/10.1016/j.corsci.2011.01.042.
- [44] Y. Peng, A.E. Hughes, J.I. Mardel, G.B. Deacon, P.C. Junk, M. Forsyth, B.R. W. Hinton, A.E. Somers, Leaching behavior and corrosion inhibition of a rare earth carboxylate incorporated epoxy coating system, Appl. Mater. Interfaces 11 (2019) 36154–36168.
- [45] N.D. Nam, A. Somers, M. Mathesh, M. Seter, B. Hinton, M. Forsyth, M.Y.J. Tan, The behaviour of praseodymium 4-hydroxycinnamate as an inhibitor for carbon dioxide corrosion and oxygen corrosion of steel in NaCl solutions, Corros Sci. 80 (2014) 128–138.
- [46] Y.-J. Tan, S. Bailey, B. Kinsella, Mapping non-uniform corrosion using the wire beam electrode method. III. Water-line corrosion, Corros. Sci. 43 (10) (2001) 1931–1937.
- [47] M. Seter, B. Hinton, M. Forsyth, Understanding speciation of lanthanum 4 hydroxy cinnamate and its impact on the corrosion inhibition mechanism for AS1020 steel, J. Electrochem. Soc. 159 (4) (2012) C181–C189.
- [48] F. Blin, S.G. Leary, G.B. Deacon, P.C. Junk, M. Forsyth, The nature of the surface film on steel treated with cerium and lanthanum cinnamate based corrosion inhibitors, Corros Sci. 48 (2) (2006) 404–419, https://doi.org/10.1016/j. corsci.2005.01.009.
- [49] M. Seter, G.M. Girard, W.W. Lee, G. Deacon, P. Junk, B. Hinton, M. Forsyth, The influence of organic structure and rare earth metal cation on the corrosion efficiency observed on AS1020 steel compared with [La(4OHcin)3].5H2O, AIMS Mater. Sci. 2 (2015) 1–15.
- [50] A.E. Somers, B.R.W. Hinton, C. deBruin-Dickason, G.B. Deacon, P.C. Junk, M. Forsyth, New, environmentally friendly, rare earth carboxylate corrosion inhibitors for mild steel, Corros. Sci. 139 (2018) 4.